ChemPubSoc Europe

DOI: 10.1002/slct.201600150

Chemistry SELECT Full Papers

Inorganic Chemistry

Coordination Behavior of Chelidamic Acid With V^{V}, Ni^{II}, Fe^{III}, and Ca^{II}: Syntheses, X-ray Characterization and DFT Studies

Milad Mahjoobizadeh,[a] Masoud Mirzaei,*[a] Antonio Bauzá,[b] Vito Lippolis,*[c] M. Carla Aragoni,[c] Mojtaba Shamsipur,[d] Manoochehr Ghanbari,[d] and Antonio Frontera*[b]

Four new complexes of chelidamic acid (H_3cda) in the presence of 2-aminopyrimidine (*apym*) or 2,4,6-triamino-1,3,5-triazine (*tata*) as external ligands, namely (*apym*H)[VO_2(H*cda*)]·H_2O (**1**), [Ni(H*cda*)(*apym*)$(H_2O)_2$]·H_2O (**2**), (*apym*H)[Fe(H*cda*)$_2$] (**3**), and (*ta-ta*H)$_2$(*tata*)$_2$[Ca_2(*cda*)$_2(H_2O)_6$]·H_2O (**4**) were synthesized. X-ray diffraction analysis of **1**-**4** revealed the formation of 3D frameworks generally involving weak interactions (mainly H-bonds) between metal complexes of chelidamic acid, protonated or deprotonated external ligands *apym* or *tata* and co-crystallized water molecules. Some complexes present remarkable assemblies in the solid state governed by unconventional non-covalent interactions that have been analyzed by means of DFT calculations. Solution studies were also performed to fully characterize the new compounds.

Introduction

In the design and synthesis of metal-organic framework (MOF) structures having potential applications as functional materials,[1] the bonding properties of the chosen ligands with binding sites in an appropriate spatial arrangement, and the stereochemical preferences of the metal ions are the most important factors to consider for controlling the topology of the ensuing products via self-assembly.[2] Weak intra- and intermolecular interactions such as H-bonding and π–π stacking interactions can also be utilized in regulating the crystallization process.[3]

In this context, pyridinedicarboxylic acids have been widely used in recent years as organic multi-dentate building blocks for the construction of organic-inorganic hybrid materials, which are of great interest due to their potential applications in many areas, such as catalysis, antibacterial activity, enzyme inhibitors, aqueous solution chemistry, surface chemistry, magnetism and fluorescence.[4,5,6]

Interestingly, while coordination polymers prepared from pyridine-2,6-dicarboxylate or dipicolinate (*dipic*$^{2-}$, Scheme 1) are

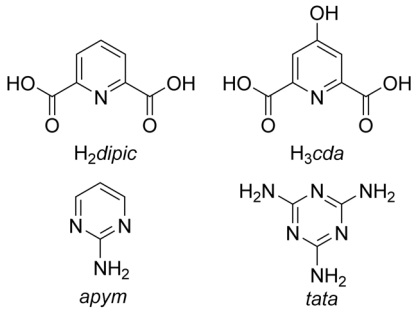

Scheme 1. Ligands considered in this work.

quite numerous,[6a,7,8,9,10] those obtained from 4-hydroxypyridine-2,6-dicarboxylate or chelidamate (H*cda*$^{2-}$, Scheme 1) are less reported[11,12,13] despite this ligand is of great interest due to its usage in many areas of sciences, including biochemistry and medical chemistry.[14] Both ligands have a rigid 120° angle between the central pyridine ring and the two carboxylic(ate) groups, thus providing various coordination motifs under appropriate synthetic conditions for main group and transition metals, and actinides. Extended structures can be achieved by supramolecular π-π stacking interactions between adjacent coordinated dipic^{2-}/H*cda*$^{2-}$ anions or by H-bonding between carboxylate oxygen acceptors and both solvent and external ligand donor O-H/N-H groups. In the case of H*cda*$^{2-}$, the phenolic O-H group is also available for H-bond networking.

Therefore, in order to extend the investigation in this field and to obtain novel extended structures based on H*cda*$^{2-}$, so to have a deeper knowledge on the coordination behavior of this ligand, we have reacted V^{3+}, Ni^{2+}, Fe^{3+} and Ca^{2+} with H_3cda in water in the presence of 2-aminopyrimidine (*apym*) or 2,4,6-tri-

[a] *M. Mahjoobizadeh, Prof. M. Mirzaei*
Department of Chemistry
Ferdowsi University of Mashhad, 917751436 Mashhad, Iran.
E-mail: mirzaeesh@um.ac.ir
[b] *A. Bauzá, Prof.Dr. A. Frontera*
Departament de Química
Universitat de les Illes Balears
Crta de Valldemossa km 7.5, 07122 Palma de Mallorca (Baleares), SPAIN
E-mail: toni.frontera@uib.es
[c] *Prof. V. Lippolis, M. C. Aragoni*
Dipartimento di Scienze Chimiche e Geologiche,.
Universita' degli Studi di Cagliari
Complesso Universitario di Monserrato, S.S. 554 Bivio per Sestu, 09042 Monserrato (CA), Italy
E-mail: lippolis@unica.it
[d] *M. Shamsipur, M. Ghanbari*
Faculty of Chemistry
Razi University
Kermanshah, Iran

Supporting information for this article is available on the WWW under http://dx.doi.org/10.1002/slct.201600150

amino-1,3,5-triazine (*tata*) as external ligands. The isolated complexes (*apym*H)[VO_2(H*cda*)]·H_2O (**1**), [Ni(H*cda*)(*apym*)(H_2O)$_2$]·H_2O (**2**), (*apym*H)[Fe(H*cda*)$_2$] (**3**), and (*tata*H)$_2$(*tata*)$_2$[Ca_2(*cda*)$_2$(H_2O)$_6$]·H_2O (**4**) were characterized by X-ray diffraction analysis. Solution studies have also been performed to understand the behavior of the ternary systems M^{n+}/H_3*cda*/*apym* (M^{n+} = VO^{2+}, Ni^{2+}, Fe^{3+}) and Ca^{2+}/H_3*apym*/*tata*.

Results and Discussion

3.1. Synthesis

Over the past decade, we have been interested in the syntheses, structural features and coordination behavior towards metal ions of proton-transfer compounds obtained by reacting organic donor ligands (D) containing N, S, and O heteroatoms and aromatic or aliphatic polycarboxylic acids, including H_2dipic and H_3*cda* (Scheme 1) (it is generally accepted that the reaction of an acid with a base will form a proton-transfer salt if the ΔpK_a = p*K*a (base) - p*K*a (acid) is greater than 2 or 3).[14d,15] The versatility of proton-transfer compounds in the construction of organized inorganic supramolecular arrays resides in their ability to act as complexing agents towards metal ions in polar solvents such as water. Furthermore, in the resulting systems, counter ion species $(DH)^+$ control the self-assembly of metal complex-organo-networks *via* simultaneous ionic and H-bonding interactions with the anionic metal complexes of the polycarboxylate ligands.

Starting, therefore, from the *in situ* preformed proton-transfer compound (*apym*H)$_2$(H*cda*) and the appropriate metal salts in 2:1 molar ratio, crystal corresponding to the formulation (H*apym*)[VO_2(H*cda*)]·H_2O (**1**), [Ni(H*cda*)(*apym*)(H_2O)$_2$]·H_2O (**2**) and (H*apym*)[Fe(H*cda*)$_2$] (**3**) were obtained from aqueous solutions after slow evaporation of the solvent. The complex (H*tata*)$_2$(*tata*)$_2$[Ca_2(H*cda*)$_2$(H_2O)$_6$]·H_2O (**4**) was also obtained following a similar procedure but starting from the preformed proton-transfer compound (*tata*H)$_2$(H*cda*). An X-ray diffraction analysis of the four complexes was undertaken to understand their nature.

X-ray crystal structure of (*apym*H)[VO_2(H*cda*)]·H_2O (1)

The molecular structure of **1** consists of one discrete mononuclear anionic complex [VO_2(H*cda*)]$^-$, shown in Figure 1, one (H*apym*)$^+$ cation fragment and one uncoordinated water molecule.

The vanadium(V) atom exhibits an overall penta-coordination with a distorted trigonal-bipyramidal geometry where equatorial coordination comes from the pyridyl nitrogen atom (N1) and two oxo ligands (O7 and O6), while two carboxylate oxygen atoms (O1 and O4) from the tridentate Hcda^{2-} ligand occupy the axial positions (Figure 1). A similar coordination environment with the VO_2 group in a *cis* configuration and the carboxylate oxygen atoms coordinated *trans* to each other, has already been observed in the previously reported V^V complexes (NMe_4)[VO_2(H*cda*)]·H_2O, K[VO_2(H*cda*)]·H_2O and Na[VO_2(H*cda*)]·2H_2O which have recently been found to have insulin-like properties.[12c,16] The V-O_{oxo} bonds (1.6228(11)/1.6249(11)Å) are significantly shorter than the V-$O_{carboxy}$ ones (1.9954(10)/2.0045(10)Å) in agreement with a double bonding with considerable π character for them.

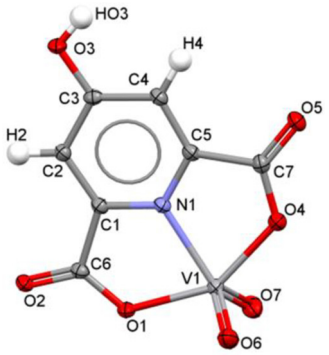

Figure 1. View of the [VO_2(H*cda*)]$^-$ metal complex in compound **1** with the atom numbering scheme adopted, displacement ellipsoids are drawn at 50% probability level. Selected bond distances and angles: V1–O6 1.6228(11), V1–O7 1.6249(11), V1–O4 1.9954(10), V1–O1 2.0045(10), V1–N1 2.0818(11) Å, O6–V1–O7 110.19(6), O6–V1–O4 98.15(5), O7–V1–O4 97.01(5), O6–V1–O1 99.74(5), O7–V1–O1 100.18(5), O4–V1–O1 149.08(4), O6–V1–N1–124.06(5), O7–V1–N1 125.71(5), O4–V1–N1 74.86(4), O1–V1–N1 74.23(4)°.

Anionic complex units [VO_2(H*cda*)]$^-$ interact head-to-tail *via* H-bonding interactions involving the phenolic O-H group of one unit and one carboxylate function of the adjacent unit to form ribbons along the *b* direction (Figure 2). These infinite ribbons are joined together by H-bonds involving both (*apym*H)$^+$ counter cations and water molecules to form infinite sheets perpendicular to the *a* direction (Figure 2) and featuring $R_2^2(8)$, $R_2^2(9)$, $R_4^4(14)$, $R_3^3(11)$ and $R_3^5(21)$ cyclic H-bonding motifs.

Sheets of this kind pack along the *a* direction in the crystal lattice and interact *via* H-bonds mainly involving the two oxo ligands at the metal center, the water molecules and the (*apym*H)$^+$ cations to complete a three-dimensional H-bonded supramolecular network (Figure 3).

X-ray crystal structure of [Ni(H*cda*)(*apym*)(H_2O)$_2$]·H_2O (2)

The structure of **2** consists of one neutral [Ni(H*cda*)(*apym*)(H_2O)$_2$] (Figure 4) complex unit and one water molecule in the asymmetric unit. The nickel(II) ion exhibits an overall hexa-coordination with a distorted octahedral geometry where equatorial coordination comes from the pyridine N atom and one O atom from each of the two carboxylates of a coordinated Hcda^{2-} anion along with one pyrimidine N atom of *apym* located in *trans*-position to the pyridine N atom of Hcda^{2-}. Two axial coordinate water molecules complete the coordination sphere. A similar coordination geometry for nickel(II) has been observed in the compound [Ni(H*cda*)(H_2O)$_3$]·1.5H_2O[17] where three water molecules are directly coordinated to the metal center.

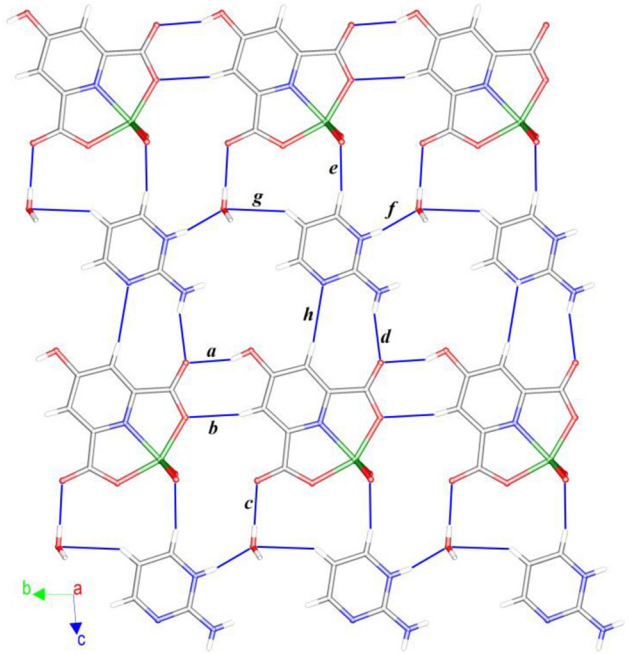

Figure 2. Partial view along crystallographic axis *a* of the extended 2D structure determined by H-bonding interactions along the (011) plane between $[VO_2(Hcda)]^-$ complex anions, $(apymH)^+$ counter cations and water molecules in the crystal structure of compound **1**. ***a***: O3–HO3···O2^{i}, 1.92, 2.7131(14), 159; ***b***: C4–H4···O1^{i}, 2.29, 3.2217(17), 167; ***c***: O1w–H1w···O5, 1.89, 2.7263(16), 171; ***d***: N4–HN4B···O2, 2.11, 2.8875(16), 159; ***e***: C11–H11···O6^{ii}, 2.44, 3.344(2), 158; ***f***: N2–HN2···O1w^{iii}, 1.84, 2.6717(19), 162; ***g***: C10–H10···O1w^{ii}, 2.60, 3.396(3), 142; ***h***: C2–H2···N3, 2.55 Å, 3.4910(19) Å, 173°. Symmetry codes: ^{i} x, 1 + y, z; ^{ii} x, y, -1 + z; ^{iii} x, -1 + y, -1 + z.

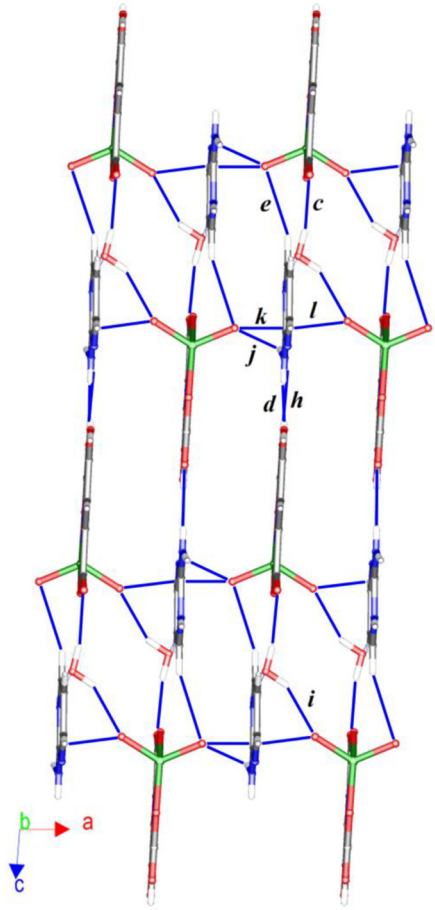

Figure 3. Partial view along *b* of the crystal packing in **1**. ***i***: O1w–H2w···O7^{iv}, 1.97, 2.7522(16), 150; ***j***: N4–HN4A···O6^{v}, 2.14, 2.8748(17), 146; ***k***: C9–H9···O6^{vi}, 2.50, 3.1710(19), 127; ***l***: C9–H9···O7^{vii}, 2.55 Å, 3.2337(19) Å, 129°. Symmetry codes: ^{iv} 1-x, 1-y, 2-z; ^{v} -x, -y, 1-z; ^{vi} -x, 1-y, 1-z; ^{vii} 1-x, 1-y, 1-z.

It is interesting to note that differently to what observed in complexes **1**, **3**, and **4**, complex **2** features a neutral *apym* unit coordinated to the nickel ion. The resulting neutral complexes pack in order to maximize both π-π interactions involving the $Hcda^{2-}$ and *apym* rings, and H-bonds (Figures 5, Table S1) involving the free and coordinated water molecules, the phenoxy OH group, the coordinated carboxylic groups, and the uncoordinated N atom of the *apym* ligand. The assembly can be described as interacting $[Ni(Hcda)(apym)(H_2O)_2]$ complex units forming corrugated sheets as that showed in Figure 5 and evidenced in monochromatic green in Figure 6. The sheets pack in the crystal lattice along the *c* direction (Figure 6).

X-ray crystal structure of (H*apym*)[Fe(H*cda*)$_2$] (3)

The molecular structure of **3** consists of one discrete mononuclear anionic complex $[Fe(Hcda)_2]^-$ and one $(apymH)^+$ cation (Figure 7). The iron(III) ion is coordinated by two $Hcda^{2-}$ anions acting as tridentate ligands in a distorted octahedral coordination geometry. The two coordinated $Hcda^{2-}$ units lay on almost perpendicular planes with Fe–O bond distances in the range 1.9992(10)-2.0695(10) Å, and almost equivalent Fe–N lengths [2.0404(11), 2.0510(12) Å].

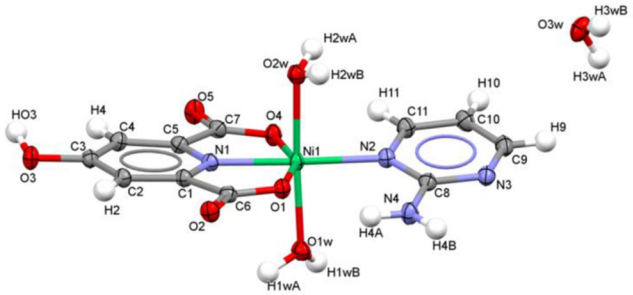

Figure 4. View of the $[Ni(Hcda)(apym)(H_2O)_2]$ complex in **2** with the atom numbering scheme adopted, displacement ellipsoids are drawn at 50% probability level. Selected bond distances and angles: Ni1–N1 1.9665(9), Ni1–N2 2.0617(9), Ni1–O1w 2.0765(8), Ni1–O2w 2.0923(8), Ni1–O4 2.1106(8), Ni1–O1 2.1274(8) Å, N1–Ni1–N2 174.78(4), N1–Ni1–O1w 93.06(3), N2–Ni1–O1w 87.64(3), N1–Ni1–O2w 89.36(3), N2–Ni1–O2w 90.53(3), O1w–Ni1–O2w 173.11(3), N1–Ni1–O4 78.79(3), N2–Ni1–O4 96.00(3), O1w–Ni1–O4 94.73(3), O2w–Ni1–O4 92.06(3), N1–Ni1–O1 77.60(3), N2–Ni1–O1 107.61(3), O1w–Ni1–O1 86.45(3), O2w–Ni1–O1 87.78(3), O4–Ni1–O1 156.40(3)°.

The packing of the complexes is governed by the numerous H-bonds engendered by the presence of several charged

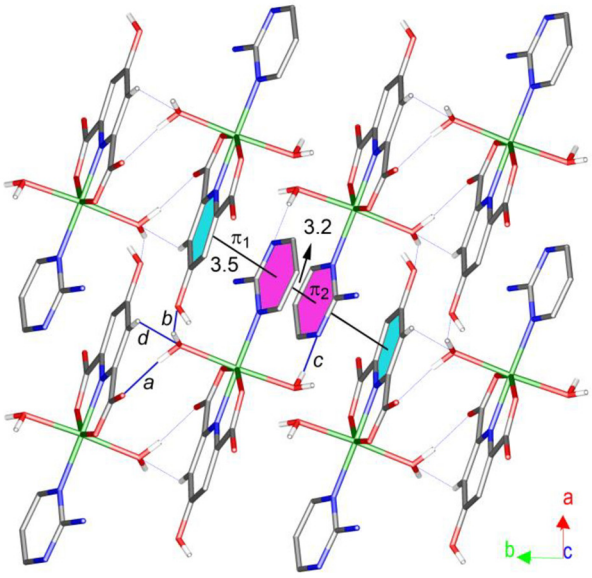

Figure 5. Partial view along *c* of the 2D supramolecular architecture of interacting [Ni(H*cda*)(*apym*)(H_2O)$_2$] complex units. ***a***: O1w–H1wA···O2^{i}, 1.77, 2.6923(13), 173; ***b***: O1w–H1wB···O3^{ii}, 1.86, 2.7558(13), 162; ***c***: O2w–H2wB···N3^{iii}, 1.84, 2.7501(13), 167; ***d***: C2–H2···O1w^{i}, 2.58 Å; 3.3839(13) Å; 143°; π_1 (H*cda*)(*apym*) 14°, $d_{interplanar}$: 3.5 Å; π_2 (*apym*)(*apym*) 0°, $d_{interplanar}$: 3.2 Å (b).

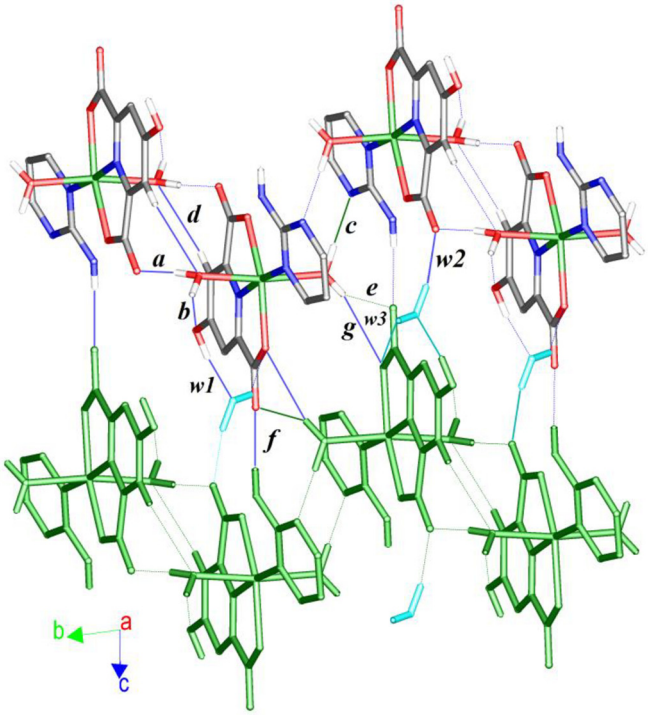

Figure 6. Partial view along *a* of the crystal packing in **2**. ***e***: O2w–H2wA···O5^{iv}, 1.93, 2.7811(13), 151; ***f***: N4–H4B···O5^{v}, 2.03, 2.9325(13), 173; ***g***: O2w–H2wA···O4^{iv}, 2.55, 3.3830(12), 149; ***w1***: O3–HO3···O3w^{iv}, 1.65, 2.5675(12), 169; ***w2***: O3w–H3wB···O2^{iii} 1.87, 2.7684(12), 160; ***w3***: O3w–H3wA···O4^{vi} 2.03 Å, 2.8439(13)Å, 144°. H-atoms not involved in the showed interactions are omitted. Non-coordinated water molecules are evidenced in monochromatic light blue. Symmetry codes: ^{i} -x, 2-y, -z; ^{ii} 1+x, y, z; ^{iii} 1-x, 1-y, -z; ^{iv} -x, 1-y, 1-z; ^{v} 1+x, y, -1+z; ^{vi} 1-x, 1-y, 1-z. .

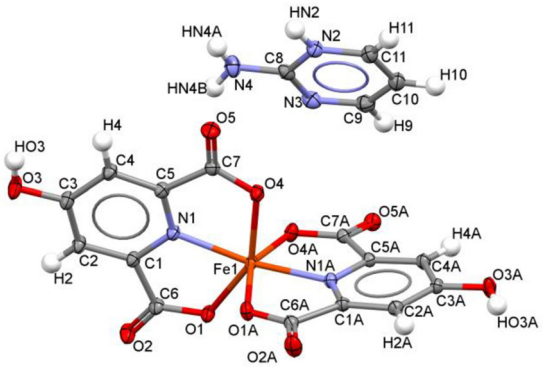

Figure 7. View of (*apym*H)[Fe(H*cda*)$_2$] (**3**) with the atom numbering scheme adopted, displacement ellipsoids are drawn at 50% probability level. Selected bond distances and angles: Fe1–O4A 1.9992(10), Fe1–O1 2.0161(10), Fe1–O1A 2.0287(11), Fe1–N1A 2.0404(11), Fe1–N1 2.0510(12), Fe1–O4 2.0695(10) Å, O4A–Fe1–O1 92.14(4), O4A–Fe1–O1A 151.46(4), O1–Fe1–O1A 94.50(4), O4A–Fe1–N1A 76.62(4), O1–Fe1–N1A 119.35(4), O1A–Fe1–N1A 75.93(4), O4A–Fe1–N1 111.20(4), O1–Fe1–N1 75.99(4); O1A–Fe1–N1 97.34(4), N1A–Fe1–N1 163.29(5), O4A–Fe1–O4 95.91(4), O1–Fe1–O4 151.00(4), O1A–Fe1–O4 91.59(4), N1A–Fe1–O4 89.63(4), N1–Fe1–O4 75.12(4)°.

and neutral functional groups (carboxylate, pyridinium, hydroxy, and amino) able to interact among each other. In the solid state architecture of **3**, the main motif can be recognized in ladders formed by symmetry related $C_1^1(7)$ chains, running along the *a* direction, made of [Fe(H*cda*)$_2$]$^-$ anionic units interacting through the strong O3A–H$_{O3A}$···O4^{i} and O3–HO3···O2^{ii} (***a*** and ***b*** in Figure 8 and Table S1) H-bonds involving the OH groups and the coordinated carboxylates.

In Figure 9 shows how the ladders (orange colored) are held together by H-bonds (***e-k*** Table S1 and Figure 9) involving both the amino and pyrimidinium N–H groups in the *apym*H cations (blue colored) and the carboxylate units of coordinated H*cda*$^-$ ligands. The amino-pyrimidinium cations and the N1A-C5A rings of the relevant H*cda*$^-$ units are also involved in π···π interactions (*apym*H)$^+$···(H*cda*)$^-$···(H*cda*)$^-$···(*apym*H)$^+$ connecting four facing parallel or almost parallel units (π_1 and π_2, Figure 9). Interestingly, **3** is isostructural to reported complexes (*apy*H)[Fe(*dipic*)$_2$] and [*acr*H][Fe(*cda*)$_2$] (*apy* = 2-aminopyridine; acr = acridine).[18]

X-ray structure of (H*tata*)$_2$(*tata*)$_2$[Ca$_2$(*cda*)$_2$(H$_2$O)$_6$]·2H$_2$O (4)

The structure of compound **4** consists of a discrete binuclear [Ca$_2$(*cda*)$_2$(H$_2$O)$_6$]$^{2-}$ complex anion, sitting on an inversion centre, in which each metal centre adopts a heptacoordinated pentagonal bipyramidal geometry (Figure 10). Two (*tata*H)$^+$ counter cations, two uncoordinated *tata* units and a water molecule complete the asymmetric unit.

The calcium ions are coordinated by a water molecule and two *cda*$^{3-}$ ligands in the equatorial plane, and two coordinated water molecules in the axial positions. The *cda*$^{3-}$ units behave as tridentate μ_2-η^2,η^1,η^1 ligands, with the heterocyclic N1 and the O4 oxygen atoms bound to metal ions and the O1 oxygen

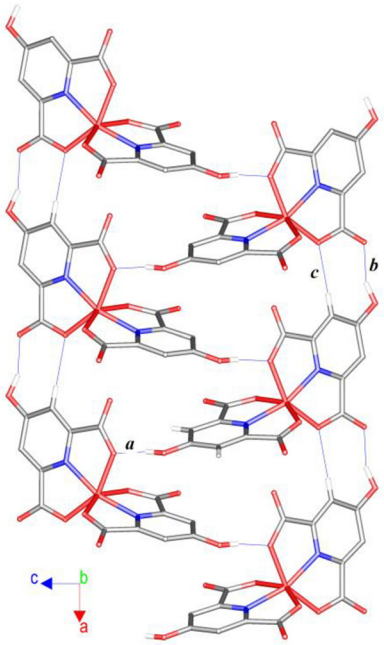

Figure 8. View along *b* of the columnar arrangement of $[Fe(Hcda)_2]^-$ units in **3** held by O–H···O H-bonds. ***a***: O3A–HO3A···O4^{i} 1.70, 2.6084(14), 174; ***b***: O3–HO3···O2^{ii} 1.75; 2.6597(15); 155; ***c***: C4–H4···O1^{ii} 2.27 Å; 3.1716(18) Å; 157°. Symmetry codes: ^{i} 0.5 + x, y, 0.5–z; ^{ii} –1 + x, y, z. Hydrogen atoms not involved in shown interactions are omitted for clarity reasons.

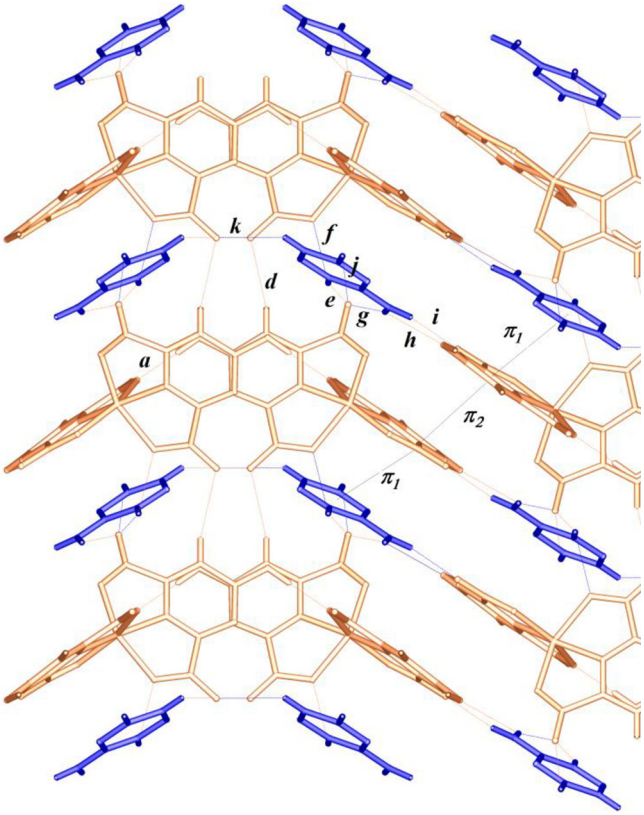

Figure 9. Packing view of **3** along axis *a* direction showing the ladders (showed in Figure 8and here evidenced in orange) made of $[Fe(Hcda)_2]^-$ anionic units interacting with *apym*H cations (blue colored) through the followings: ***a***: O3A–HO3A···O4^{i} 1.70, 2.6084(14), 174; ***d***: C4A–H4A···O2A^{iii} 2.51, 3.4068(17), 157; ***e***: N2–HN2···O5A^{ii} 1.91, 2.7661(17), 153; ***f***: N2–HN2···O1A^{iv} 2.59, 2.9974(16), 107; ***g***: N4–HN4A···O5A^{ii} 2.08, 2.8887(17), 147; ***h***: N4–HN4A···O3^{v} 2.58, 3.0418(17), 112; ***i***: N4–HN4B···O2^{vi} 1.96, 2.8342(17), 147; ***j***: C9–H9···O5A 2.51, 3.1452(19), 125; ***k***: C10–H10···O2A^{vii} 2.47 Å, 3.0801(19) Å, 122°; π_1 $(Hcda)^-$ $(apymH)^+$ 14°, $d_{interplanar}$: 3.5 Å; π_2 $(Hcda)^-$ $(Hcda)^-$ 0°, $d_{interplanar}$: 3.4 Å Symmetry codes: ^{i} 0.5 + x, y, 0.5–z; ^{ii} –1 + x, y, z; ^{iii} 1.5–x, 0.5 + y, z; ^{iv} 0.5–x, 0.5 + y, z; ^{v} –x, –y, –z; ^{vi} 1–x, –y, –z; ^{vii} 1–x, 0.5 + y, 0.5–z. Hydrogen atoms not involved in shown interactions are omitted for clarity reasons.

atoms bridging the calcium ions [Ca–O1 2.3956 (19), Ca1–O1′ 2.4792(18) Å] (Figure 10). The phenolic O-H groups are deprotonated, an unusual feature for metal complexes of chelidamic acid, which has been already observed in two of the four *cda* units of the complex $(H_2daprop)_2$ $[Ca_2(Hcda)_2(cdaH)_2(H_2O)_2]\cdot 2H_2O$ (*daprop* = 1,3-diaminopropane). In this case the two metal centers are bridged *via* four chelidamic units: two feature a protonated O-H function and bind the two metal centers as in **4**, the other two take the place of the four axial water molecules in **4** and bridge the two metal centers through the carboxylate groups with an internal proton transfer from the phenolic functions to the pyridine nitrogen atoms, which therefore, are not coordinated to the metal.[19]

$[Ca_2(cda)_2(H_2O)_6]^{2-}$ units interact each other via Ow–Hw···O H-bonds involving the coordinated water molecules (see Table S1, Figure S3) and the phenolate oxygen atoms to give 2D assemblies in the (110) plane (Figure 11).

Triaminotriazine units interact via N–H···N H-bonds to form ribbons along the [110] direction which stack along the [1-10] direction (Figure 12).

The crystal packing of **4** is built by an alternate disposition along *c* of sheets of $[Ca_2(cda)_2(H_2O)_6]^{2-}$ anionic units (yellow colored in Figure S3) and stacks of triaminotriazine units (yellow colored in Figure S3) held together via H-bonds mainly involving the uncoordinated water molecules (red colored in Figure S3).

Theoretical study

We have analyzed the noncovalent interactions observed in the solid state of compounds **1–4** energetically focusing our attention to the anion–π, π–hole and antiparallel π–π interactions. Particularly π–hole interactions are increasing attention in supramolecular chemistry and crystal engineering fields.[20]

In the crystal structure of compound **1** we have observed an interesting assembly (see Figure 13A) where the anionic $[VO_2(Hcda)_2]^-$ complex and the aminopyrimidinium cation (*apym*H) ion-pair are antiparallel stacked to other ion pairs forming infinite columns. Interestingly, the H*cda* ligand is stacked to the H-bonding array resembling a salt-bridge···π interaction. We have computed the Molecular Electrostatic Potential Surface (MEPS) of $(apymH)[VO_2(Hcda)_2]$ ion-pair to investigate the positive and negative regions and rationalize the interactions (see Figure 13B xfigr13>). The most positive region corresponds to the N–H that establishes an H-bond with the lattice water molecules. It can be observed a positive re-

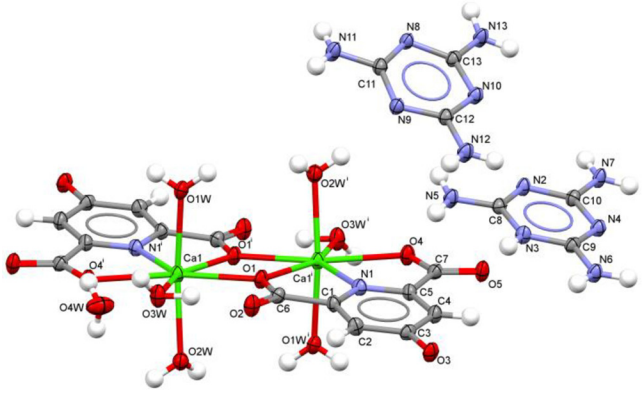

Figure 10. View of $(tataH)_2(tata)_2[Ca_2(cda)_2(H_2O)_6]\cdot 2H_2O$ (**4**) with the atom numbering scheme adopted, displacement ellipsoids are drawn at 50% probability level. Selected bond distances and angles: Ca–O1 2.3956 (19); Ca1–O1W 2.354(2), Ca1–O2W 2.364(2), Ca1–O4^{i} 2.3998(18), Ca1–O3W 2.417(2), Ca1–N1^{i} 2.428(2), Ca1–O1^{i} 2.4792(18), Ca1–Ca1^{i} 3.9244(10) Å, O1W–Ca1–O2W 171.20(7), O1W–Ca1–O1 84.79(7), O2W–Ca1–O1 88.18(7), O1W–Ca1–O4^{i} 95.49(7), O2W–Ca1–O4^{i} 88.88(7), O1– Ca1–O4^{i} 156.81(6), O1W–Ca1–O3W 87.68(7), O2W–Ca1–O3W 86.07(7), O1–Ca1–O3W 81.85(6), O4–Ca1–O3W^{i} 75.00(6), O1W–Ca1–N1^{i} 89.49(7), O2W–Ca1–N1^{i} 99.27(7), O1–Ca1–N1^{i} 137.39(7), O4 ^{i}–Ca1–N1^{i} 65.74(6), O3W–Ca1–N1^{i} 140.17(7), O1W–Ca1–O1^{i} 90.57(6), O2W–Ca1–O1^{i} 92.42(7), O1–Ca1–O1^{i} 72.79(6), O4^{i}–Ca1–O1^{i} 130.33(6), O3W–Ca1–O1^{i} 154.63(6), N1^{i}–Ca1–O1^{i} 65.07(6), O1W–Ca1–Ca1^{i} 87.18(5), O2W–Ca1–Ca1^{i} 90.42(5), O1–Ca1–Ca1^{i} 37.12(4), O4^{i}–Ca1–Ca1^{i} 165.93(5), O3W–Ca1–Ca1^{i} 118.96(5), N1^{i}–Ca1–Ca1^{i} 100.54(5), O1^{i}–Ca1–Ca1^{i} 35.67(4)°. Symmetry code: ^{i} 2-x, 1-y, 1-z.

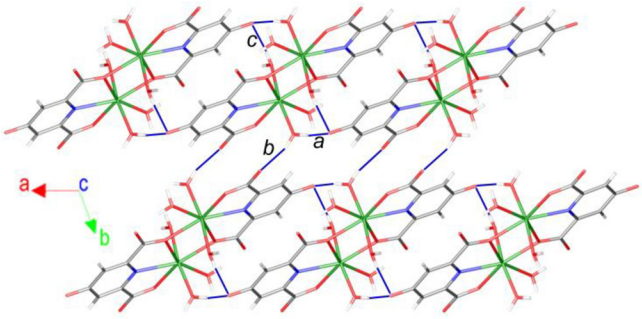

Figure 11. View along *c* of 2D assembly of $[Ca_2(cda)_2(H_2O)_6]^{2-}$ anionic units in **4** interacting *via* Ow–Hw···O H-bonds. ***a***: O1w–H1wA···O3^{ii} 1.75; 2.653(3); 170; ***b***: O1w–H1wB···O5^{iii} 1.85; 2.637(3); 159; ***c***: O2w–H2wB···O3^{iv} 1.90 Å; 2.683(3) Å; 176°. Symmetry codes: ^{ii} 1–x, 1–y, 1–z; ^{iii} 1 + x, 1 + y, z; ^{iv} 1 + x, y, z.

gion over the π-system of the *apym*H ring, thus it is well suited for interacting with anions. In contrast, the electrostatic potential over the π-system of H*cda* ring is negligible. The most negative part is in the O atoms of the VO_2 moiety and the carboxylate groups. We have computed the interaction energy $\Delta E_1 = -78.2$ kcal/mol) of the self-assembled supramolecular dimer of ion pairs (see Figure 13C), which is very large and negative due to the smart combination of several interactions (anion–π, π–π and HB). These interactions have been characterized using the Bader's theory of "atoms in molecules" (AIM). The presence of a bond critical point and a bond path connecting two atoms is an unequivocally indication of interaction. The distribution of

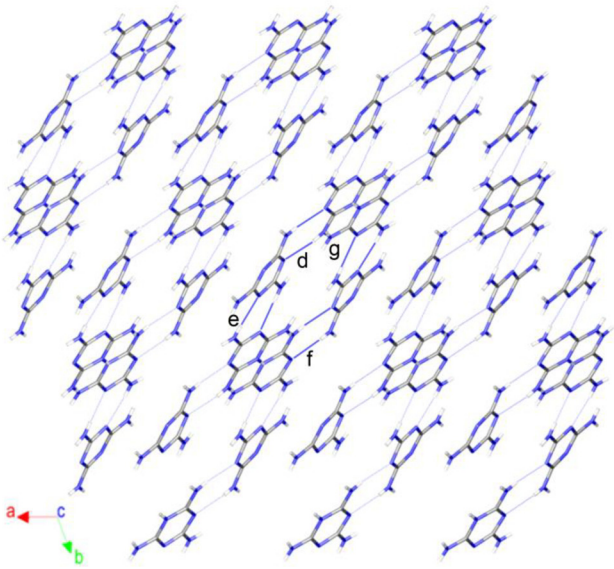

Figure 12. View along *c* of H-bonded ribbons of triaminotriazine units in **4** stacked along the [1-10] direction. ***d***: N5–H5B···N8^{v} 2.24; 3.063; 171°; ***e***: N7–H7B···N10^{vi} 2.18; 3.005(3); 177°; ***f***: N11–H11B···N2^{v} 2.24 Å; 2.999(3) Å; 172°; ***g***: N13–H13B···N4^{vi} 2.15 Å; 2.980(3) Å; 178°. Symmetry codes: ^{v} 2–x, 1–y, 2–z; ^{vi} 1–x, –y, 2–z.

critical points (CP) and bond paths of the dimer is shown in Figure 13D. This distribution shows that the dimer presents two hydrogen bonds between the VO_2^{2+} moiety and one H atom of the *apym*H ring. Each H-bond is characterized by a bond CP (red sphere) that connects the O atom to the H atom. Moreover, two symmetrically equivalent anion–π interactions are also established between the coordinated carboxylate group and the *apym*H π-system. Each interaction is characterized by the presence of three CPs that connect the three atoms of the R–COO^- group to three atoms of the *apym*H ring. The presence of this interaction agrees well with the MEP analysis, since the MEP value over the *apym*H is large and positive and negative in the region of the carboxylate (see Figure 13B). Finally, the π–π interaction is characterized by the presence of three bond CPs that connect both H*cda* rings. The arrangement of the rings in the π–π interaction also agrees well with the MEP analysis commented above, since the MEP over this ring is small, thus reducing the electrostatic repulsion and consequently, other contributions like dispersion and polarization terms can dominate the π–π interaction.

In the crystal structure of compound **2** we have observed the formation of an infinite ladder (see Figure 14A) as a consequence of the electrostatically favored stacking interactions between the $[Ni(Hcda)(apym)(H_2O)_2]$ complexes combined with H-bonds established between the coordinated water molecules as acceptors (C–H···OH_2) and donors (HOH···O). The π-interaction is established between the H*cda* and *apym* rings. We have rationalized this fact by computing the MEP surface (see Figure 14B). The most positive region corresponds to the H atoms of the coordinated water molecules. It can be also observed that the MEP over the π-system of the *apym* ring is pos-

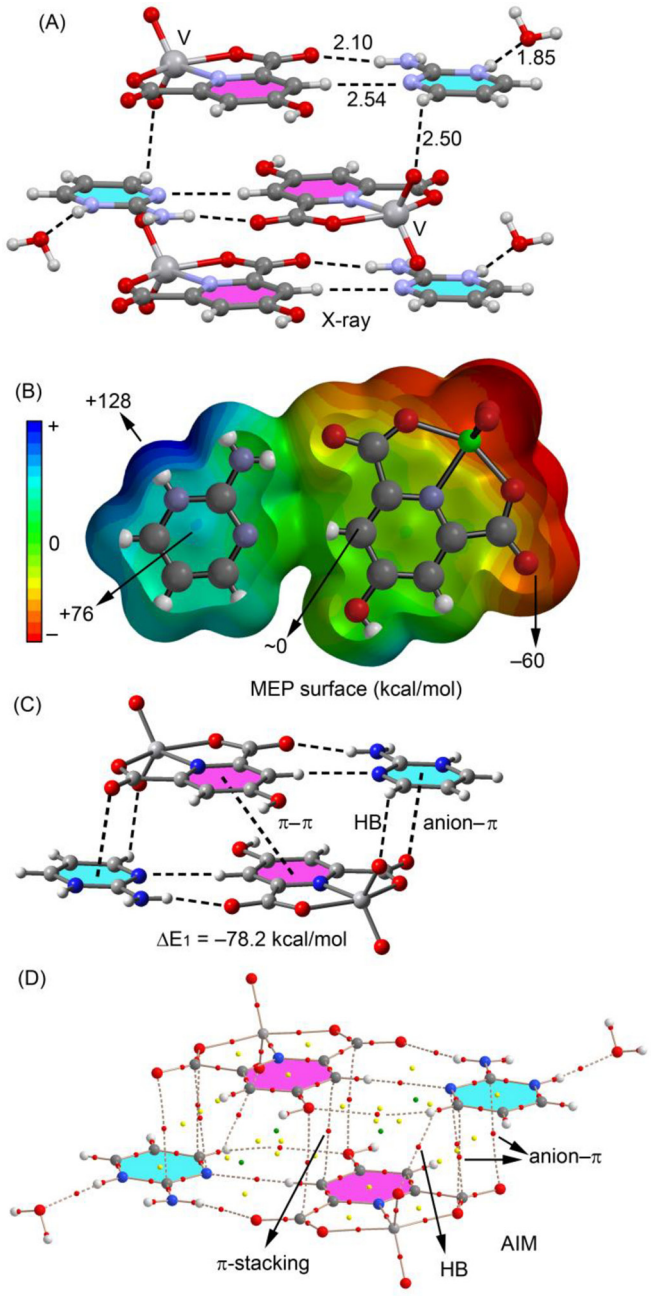

Figure 13. A) X-ray fragment of compound **1**. B) MEP surface of the ion pair. C) Theoretical model used to evaluate the noncovalent interactions. D) AIM distribution of bond (red spheres), ring (yellow spheres) and cage (green spheres) critical points. The bond paths are also represented.

itive due to the coordination to the metal center that enhances the π-acidity of the ring. Moreover, the electrostatic potential over the π-system of H*cda* ring is small but negative. Therefore the stacking observed in the solid state is electrostatically favored. We have computed the interaction energy of one dimer extracted from this infinite ladder ($\Delta E_2 = -15.3$ kcal/mol, see Figure 14C), which is large and negative due to the combination of π–π and HB interactions. The H-bonding interaction between the water molecule and the OH phenolic group is very short (1.86 Å) due to the enhanced acidity of the H atoms of the coordinated water molecule (see MEP value in Figure 14B). In an effort to evaluate the contribution of this H-bond, we have computed an additional model (see Figure 14D) where the OH group has been replaced by an H atom, and consequently this H-bond is not established. As a consequence the interaction energy is reduced to $\Delta E_3 = -6.3$ kcal/mol and the contribution of this H-bond can be estimated by difference, i.e. $\Delta E_2 - \Delta E_3 = -9.0$ kcal/mol. The AIM distribution of CPs is shown in Figure 13E. Each H-bond is characterized by a bond CP (red sphere) that connects the O atom to the H atom. Moreover, the π–π interaction is characterized by the presence of two bond CPs that connects both aromatic rings. This interaction is further characterized by the presence of a ring CP (yellow sphere) due to the formation of a supramolecular ring.

In the crystal structure of compound **3** we have observed the formation of an infinite column (see Figure 15A) as a consequence of the interaction of the (*apym*H)[Fe(H*cda*)$_2$] ion-pair with the adjacent ion pair by means of two H-bonds and a π-hole interaction. Interestingly, the π-hole interaction is established between the O atom of the carboxylate group of one ion-pair and the C atom of the coordinated carboxylate group of the other ion-pair. The O···C distance (2.88 Å) is considerably shorter than the sum of van der Walls radii (3.22 Å). We have computed the interaction energy of a dimer extracted from the infinite column (Figure 15B), which is very favorable ($\Delta E_4 = -32.0$ kcal/mol) due to the combination of π–hole and two HB interactions. We have also computed another theoretical model where we have modified the aromatic ring of one H*cda* ligand (see Figure 15C), and consequently both H-bonds are not established. As a consequence the interaction energy is reduced to $\Delta E'_4 = -17.3$ kcal/mol. This interaction energy is too large compared to the reported π-hole interactions. To further investigate this issue, we have characterized the dimer using the Bader's theory of "atoms in molecules" (AIM), see Figure 14D. The distribution of CPs demonstrates the existence of the H-bond and π-hole interactions described above (each one characterized by a bond CP). Moreover, the AIM also reveals the presence of an additional H–bond between an H-atom of the cationic *apym*H ring and an O-atom of the anionic complex. This interaction further contributes to the stabilization of the assembly and explains the large $\Delta E'_4$ interaction energy.

Finally, in complex **4**, we have analyzed the H-bonding network that is responsible of the formation of the interesting assembly in the solid state, represented in Figure 16A. The anionic dinuclear complex $[Ca_2(H\textit{cda})_2(H_2O)_6]^{2-}$ and the counterions $(H\textit{tata})^+$ interact with neutral *tata* molecules by the simultaneous formation of four H-bonds. We have evaluated the interaction energy of thisassembly that is $\Delta E_5 = -20.1$ kcal/mol using the reaction shown in Figure 16B. Therefore the interaction corresponds to the contribution of the four H-bonds. Interestingly, the protonated ligands $(H\textit{tata})^+$, which also form H bonding interactions with the dianionic complex, participate in π-hole bonding interactions (represented by red dashed lines in Figure 16). The lone pair of the amino group is located exactly over the C atom of the Ca^{2+}-coordinated carboxylate group at 2.99 Å (less than the sum of van der Waals radii). The AIM dis-

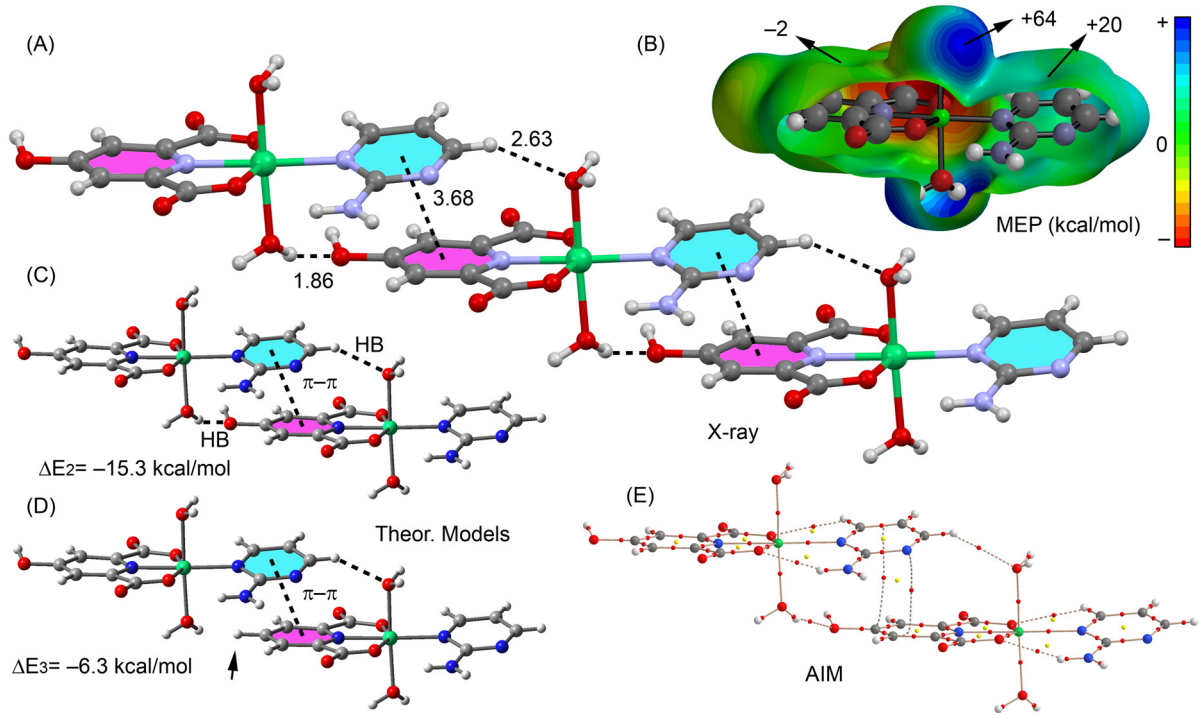

Figure 14. A) X-ray fragment of compound **2**. B) MEP surface of the ion pair. C and D) Theoretical models used to evaluate the noncovalent interactions. E) AIM distribution of bond (red spheres) and ring (yellow spheres) critical points. The bond paths are also represented.

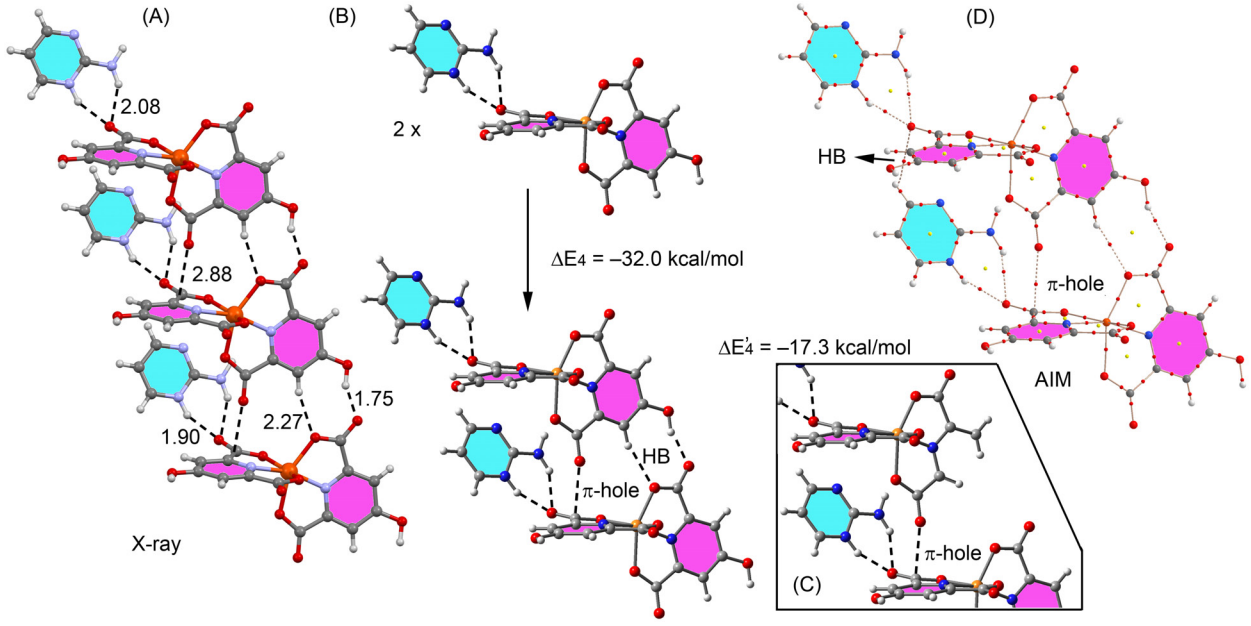

Figure 15. A) X-ray fragment of compound **3**. B and C) Theoretical model used to evaluate the noncovalent interactions. (D) AIM distribution of bond (red spheres) and ring (yellow spheres) critical points. The bond paths are also represented.

tribution of CPs confirms the existence of this interaction since one bond CP connects the N atom to the C atom of the CO_2–Ca group (see Figure 16C)

Solution studies

In order to evaluate the stoichiometry and stability of the ternary Fe^{3+} and Ni^{2+} complexes with *apym*/H_3*cda* and the ternary Ca^{2+} complex with *tata*/H_3*cda* in aqueous solution, known

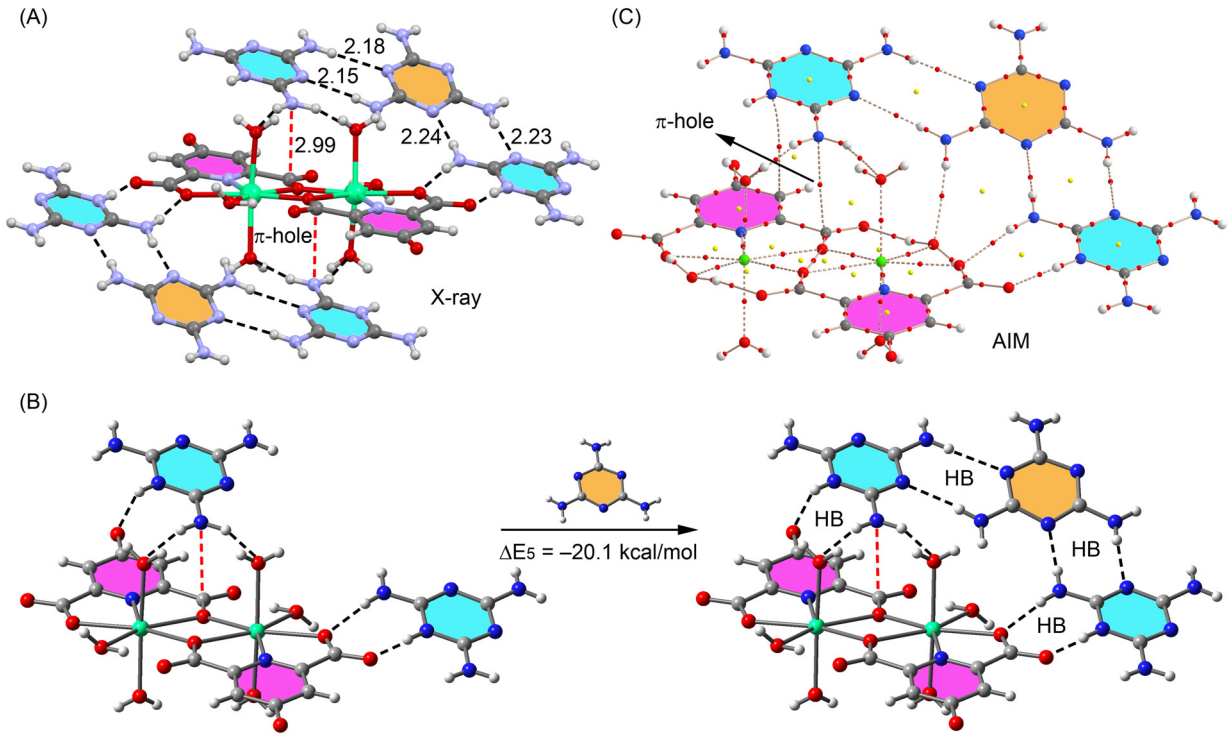

Figure 16. A) X-ray fragment of compound **4**. B) Theoretical model used to evaluate the noncovalent interactions. C) AIM distribution of bond (red spheres) and ring (yellow spheres) critical points. The bond paths are also represented.

concentrations of fully protonated ligands and their 1:1 mixtures in the absence and presence of the metal ions were titrated with a 0.099 M solution of NaOH at 25 °C, while an ionic strength of 0.1 M was maintained by $NaClO_4$. Titration continued before precipitation. Similar studies were performed for VO^{2+} (using VCl_3 as starting salt) but hydrolysis of the oxocation in the experimental conditions used prevented the investigation. It was found that H_3cda has good interaction with metal ions, because the potentiometric titration curves were depressed considerably in the presence of the metal ions (see SI, Figures S4-S6).

The extent of depression obviously depends both on the stoichiometry of resulting complexes and the ability of the metal ion to bind the ligand components. The cumulative stability constants, β_{mlqh}, are defined by Eq. (1) (charges are omitted for simplicity)

$$mL + lL + qQ + hH \leftrightarrow M_mL_lQ_qH_h \quad \beta_{mlqh}$$

$$\beta_{mlqh} = [M_mL_lQ_qH_h]/[M]^m[L]^l[Q]^q[H]^h$$

Where M is Ni^{2+}, Ca^{2+} or Fe^{3+} ions, L is H*cda* $^{2-}$, Q is *apym* or *tata* and H is proton, and m, l, q, and h are the respective stoichiometric coefficients. Since the ligand and complex activity coefficients are unknown, the β_{mlqh} values are defined in terms of concentrations. The errors are minimized by using a high-constant ionic strength of 0.1 M and low ligand concentrations (in the order of 10^{-3} M).

The potentiometric pH titration profiles of H_3cda, *apym* and their 1:1 mixture in the presence of Ni^{2+} (1 equiv.) and Fe^{3+} (0.5 equiv.) ions, and H_3cda, *tata* and their 1:1 mixture in the presence of Ca^{2+} ions (1 equiv.), were fitted with the program BEST,[27] and the calculated stability constants for the most likely complexed species in aqueous solution are reported as supplementary materials.

Evaluated acidity constants of chelidamic acid at 25 °C with BEST program (10.89, 2.9 and 2.01) agrees with results reported in the literature (see Table S2, SI).[21,22] In the case of Ni^{2+}, calculated stability constants, logβ of 1:1 and 1:2 complexes with H*cda*$^{2-}$ were 8.62 and 16.44 respectively, agrees with values previously reported, 9.2 and 17.3.[23] Sample species distribution diagram for L/Q mixtures in presence of Ni^{2+}, Ca^{2+} and Fe^{3+} are shown in Figure 17.

The percent is based on abundance of species relative to abundance of (H*cda*)$^{2-}$ (L). It is obvious from Figure 17 and Tables S3-S5 in the SI that in all three cases, among the evaluated species in solution there are also those corresponding to the complexes isolated in the solid state.

These titration studies are in good agreement with previous results available in the literature for [*acr*H][Fe(*cda*)][18b] and [9*a*-*acr*H]$_2$[Ni(*cda*)$_2$] (9*a*-*acr* = 9-amineacridine).[24]

Conclusions

In conclusion, a series of complexes with chelidamic acid, the mononuclear (*apym*H)[VO_2(H*cda*)]·H_2O (**1**), [Ni(H*cda*)(*apym*)(H_2

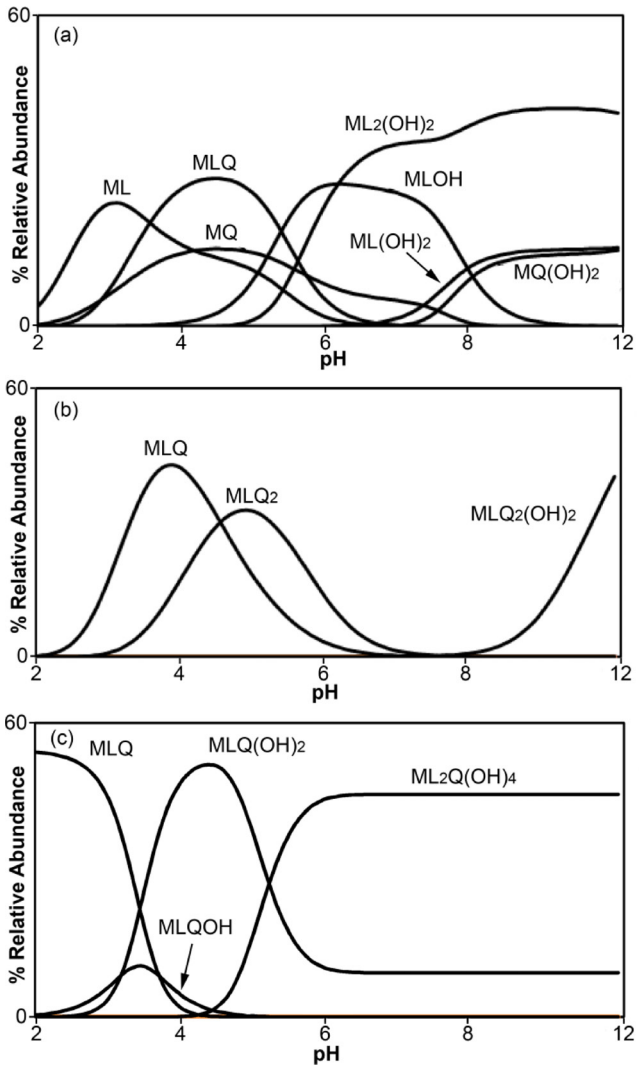

Figure 17. Species distribution diagram for (a) H*cda* $^{2-}$ (L), *apym* (Q), Ni^{2+} (M); (b) H*cda* $^{2-}$ (L), *tata* (Q), Ca^{2+} (M); (c) H*cda* $^{2-}$ (L), *apym* (Q), Fe^{3+} (M) at 25°C and ionic strength 0.1 M $NaClO_4$ in aqueous solution. In the case of Ni^{2+}, binary and ternary species are reported.

$O)_2]\cdot H_2O$ (**2**), (*apym*H)[Fe(H*cda*)$_2$] (**3**) and the binuclear (*tata*H)(*tata*)[Ca_2(H*cda*)$_2$(H_2O)$_6$]·H_2O (**4**) were obtained from aqueous solutions after slow evaporation of the solvent starting from preformed proton-transfer compounds (*apym*H)$_2$(H*cda*) or (*tata*H)$_2$(H*cda*). The crystal structures of the **1**, **2**, **3** and **4**, show that the anionic (H*cda*)$^{2-}$ or (*cda*)$^{3-}$ ligands chelate the metal atoms in a tridentate manner, by a pyridine nitrogen atom and two oxygen atoms from carboxylate groups. The observed metal-to-(H*cda*)$^{2-}$ stoichiometries are 1:2 in the case of the iron(II) complex **3**, and 1:1 in the cases of the complexes **1** and **2** in which the metal centres complete their coordination environment with either oxo groups (**1**) or water molecules and a neutral *apym* molecule (**3**). Only in the case of complex **4**, a 1:1 stoichiometry corresponds to the formation of a binuclear assembly in which two carboxylate groups of each coordinated (*cda*)$^{3-}$ unit bridge two hepta-coordinated Ca^{2+} ions, water molecules completing the coordination sphere. The different stoichiometries and charges of the obtained metal complexes balanced by (*apym*H)$^+$ (**1**, **3**) or (*tata*H)$^+$ (**4**) cations are reflected in different crystal packings and structural architectures observed in the solid state which are determined mainly by H-bonding interactions between anions and cations but also H-bonding interactions involving uncoordinated water molecules and in the case of **4**, neutral *tata* units. These results confirm the versatility of chelidamic acid together with the most known dipicolinic acid as multi-dentate building blocks for the construction of organic-inorganic hybrid materials. Finally, the influence of unconventional noncovalent interactions (π-hole) have been analyzed energetically using DFT calculations and confirmed using the Bader's theory of AIM.

Acknowledgements

The authors thank to the Ferdowsi University of Mashhad and The Fondazione Banco di Sardegna for financial support of this work (Grant No. P/2106). A.B. and A.F. thank DGICYT of Spain (projects CTQ2014-57393-C2-1-P and CONSOLIDER INGENIO CSD2010–00065, FEDER funds) for funding. We thank the CTI (UIB) for free allocation of computer time.

Keywords: MOFs · X-ray structures · Crystal structure · Solution studies · DFT calculations

[1] a) R. J. Kuppler, D. J. Timmons, Q.-R. Fang, J.-R. Li, T. A. Makal, M. D. Young, D. Yuan, D. Zhao, W. Zhuang, H.-C. Zhou, *Coord. Chem. Rev.*, **2009**, *253*, 3042-3066; b) Z. Ma, B. Multon, *Coord. Chem. Rev.*, **2011**, *255*, 1623-1641; c) Z.-Y. Gu, C.-X. Yang, N. Chang, X.-P. Yan, *Acc. Chem. Res.*, **2012**, *45*, 734-745; d) H.-L. Jiang, T. A. Makal, H.-C. Zhou, *Coord. Chem. Rev.*, **2013**, *257*, 2232-2249.

[2] a) D. Zhao, D. J. Timmons, D. Yuan, H.-C. Zhou, *Acc. Chem. Res.*, **2011**, *44* 123-133; b) M. Du, C.-P. Li, C.-S. Liu, S.-M. Fang, *Coord. Chem. Rev.*, **2013**, *257*, 1282-1305; c) J. J. Perry IV, J. A. Perman, M. J. Zaworotko, *Chem. Soc. Rev.*, **2009**, *38*, 1400-1417; d) S. Qiu, G. Zhu, *Coord. Chem. Rev.*, **2009**, *253*, 2891-2911.

[3] a) I. A. Baburin, V. A. Blatov, L. Carlucci, G. Ciani, D. M. Proserpio, *CrystEngComm*, **2008**, *10*, 1822-1838; b) D. Braga, F. Grepioni, G.R. Desiraju, *Chem. Rev.*, **1998**, *98*, 1375-1405.

[4] A. T. Colak, O. Z. Yesilel, O. Büyükgüngör, *Polyhedron*, **2010**, *29*, 2127-2133.

[5] H. Eshtiagh-Hosseini, M. Mirzaei, M. Biabani, V. Lippolis, M. Chahkandi, C. Bazzicalupi, *CrystEngComm*, **2013**, *15*, 6752-6768.

[6] J. Lü, E. Shen, Y. Li, D. Xiao, E. Wang, L. Xu, *Cryst. Growth Des.*, **2005**, *5*, 65-67.

[7] a) B. Zhao, X.-Y. Chen, P. Cheng, D.-Z. Liao, S.-P. Yan, Z.-H. Jiang, *J. Am. Chem. Soc.*, **2004**, *126*, 15394-15395; b) S. K. Ghosh, P. K. Bharadwaj, *Inorg. Chem.*, **2005**, *44*, 5553-5555; c) S. K. Ghosh, P. K. Bharadwaj, *Inorg. Chem.*, **2004**, *43*, 2293-2298; d) S. K. Ghosh, J. Ribas, P. K. Bharadwaj, *Cryst. Growth Des.*, **2005**, *5*, 623-629.

[8] a) X.-Q. Zhao, B. Zhao, Y. Ma, W. Shi, P. Cheng, Z.-H. Jiang, D.-Z. Liao, S.-P. Yan, *Inorg. Chem.*, **2007**, *46*, 5832-5834; b) S. K. Ghosh, P. K. Bharadwaj, *Inorg. Chem.*, **2005**, *44*, 3156-3161; c) L. Wen, Y. Li, Z. Lu, J. Lin, C. Duan, Q. Meng, *Cryst. Growth Des.*, **2006**, *6*, 530-537; d) T. K. Prasad, M. V. Rajasekharan, *Inorg. Chem.*, **2009**, *48*, 11543-11550; e) V. Chandrasekhar, C. Mohapatra, R. J. Butcher, *Cryst. Growth Des.*, **2012**, *12*, 3285-3295.

[9] a) M. Felloni, A. J. Blake, P. Hubberstey, C. Wilson, M. Schröder, *Cryst. Growth Des.*, **2009**, *9*, 4685-4699; b) S. C. Manna, E. Zangrando, N. R. Chaudhuri, *J. Mol. Struct.*, **2008**, *877*, 145-151; c) B. Das, J. B. Baruah, *Polyhedron*, **2012**, *31*, 361-367; d) N.-H. Hu, Z.-G. Li, J.-W. Xu, H.-Q. Jia, J.-J. Niu, *Cryst. Growth Des.*, **2007**, *7*, 15-17; e) V. A. Milway, V. Neil, T. S. M. Abedin, Z. Xu, L. K. Thompson, H. Grove, D. O. Miller, S. R. Parsons, *Inorg.*

Chem., **2004**, *43*, 1874-1884; f) M.O. Rodrigues, J. D. Lisboa Dutra, G. F. de Sá, W. M. de Azevedo, P. Silva, F. A. Almeida Paz, R. Oliveira Freire, S. A. Júnior, *J. Phys. Chem. C*, **2012**, *116*, 19951-19957.

[10] a) S.K. Ghosh, J. Ribas, P. K. Bharadwaj, *CrystEngComm*, **2004**, *6*, 250-256; b) S.C. Manna, J. Ribas, E. Zangrando, N.R. Chaudhuri, *Inorg. Chim. Acta*, **2007**, *360*, 2589-2597; c) S. Cui, Y. Zhao, J. Zhang, Q. Liu, Y. Zhang, *Cryst. Growth Des.*, **2008**, *8*, 3803-3809; d) M. Mirzaei, H. Eshtiagh-Hosseini, V. Lippolis, H. Aghabozorg, D. Kordestani, A. Shokrollahi, R. Aghaei, A.J. Blake, *Inorg. Chim. Acta*, **2011**, *370*, 141-149.

[11] a) M. Mirzaei, V. Lippolis, M. C. Aragoni, M. Ghanbari, M. Shamsipur, F. Meyer, S. Demeshko, S. M. Pourmortazavi, *Inorg. Chim. Acta*, **2014**, *418*, 126-135; b) H. Eshtiagh-Hosseini, M. Mirzaei, *Mendeleev Commun.*, **2012**, *22*, 323-324; c) M. Mirzaei, H. Eshtiagh-Hosseini, Z. Karrabi, B. Notash, A. Bauzá, A. Frontera , *J. Mol. Struct.*, **2015**, *1080*, 30-36; d) D. Saha, T. Maity, S. Koner, *Dalton Trans.* **2014**, *43*, 13006-13017; e) D. Saha, T. Maity, S. Koner, *Eur. J. Inorg. Chem.* **2015**, 1053-1064.

[12] a) H.-L. Gao, L. Yi, B. Zhao, X.-Q. Zhao, P. Cheng, D.-Z. Liao, S.-P. Yan, *Inorg. Chem.*, **2006**, *45*, 5980-5988; b) J.-P. Zou, Q. Peng, Z. Wen, G.-S. Zeng, Q.-J. Xing, G.-C. Guo, *Cryst. Growth Des.*, **2010**, *10*, 2613-2619; c) L. Yang, A. la Cour, O. P. Anderson, C. Crans, *Inorg. Chem.*, **2002**, *41*, 6322-6331; d) S. K. Gosh, S. Neogi, E. C. Sanudo, P.K. Bharadwaj, *Inorg. Chim. Acta*, **2008**, *361*, 56-62.

[13] a) H.-L. Gao, B. Zhao, X.-Q. Zhao, Y. Song, P. Cheng, D.-Z. Liao, S.-P. Yan, *Inorg. Chem.*, **2008**, *47*, 11057-11061; b) J.-P. Zou, G.-W. Zhou, X. Zhang, M.-S. Wang, Y.-B. Lu, W.-W. Zhou, Z.-J. Zhang, G.-C. Guo, J.-S. Huang, *CrystEngComm*, **2009**, *11*, 972-974; c) M. Mirzaei, V. Lippolis, H. Eshtiagh-Hosseini, M. Mahjoobizadeh, *Acta Crystallogr., Sect. C*, **2012**, *68*, m7-m11; d) H. Eshtiagh-Hosseini, M. Mirzaei, S. Zarghami, A. Bauzá, A. Frontera, J. T. Mague, M. Habibi, M. Shamsipur, *CrystEngComm*, **2014**, *16*, 1359-1377; e) M. Mirzaei, H. Eshtiagh-Hosseini, Z. Karrabi, B. Notash, *Acta Crystallogr., Sect. C*, **2013**, *69*, 1140-1143; f) M. F. Belian, W. E. Silva, G. F. de Sá, S. Alves Jr. , R. F. de Farias, *Synth. React. Inorg. Met.-Org. Nano-Met. Chem.*, **2014**, *44*, 1461.

[14] a) D.L. Boger, J. Hong, M. Hikota, M. Ishida, *J. Am. Chem. Soc.*, **1999**, *121*, 2471-2477; b) T. Fessmann, J.D. Kilburn, *Angew. Chem., Int. Ed. Engl.*, **1999**, *38*, 1993-1996; c) M. Searcey, S. McClean, B. Madden, A.T. McGown, L.P.G. Wakelin, *Anti-Cancer Drug. Des.*, **1998**, *13*, 837-855; d) M. Mirzaei, H. Aghabozorg, H. Eshtiagh-Hosseini, *J. Iran. Chem. Soc.*, **2011**, *8*, 580-607.

[15] H. Aghabozorg, F. Manteghi, S. Sheshmani, *J. Iran. Chem. Soc.*, **2008**, *5*, 184.

[16] D. C. Crans, M. Mahroof-Tahir, M. D. Johnson, P. C. Wilkins, L. Yang, K. Robbins, A. Johnson, J. A. Alfano, M. E. Godzala, L. T. Austin, G. R. Willsky, *Inorg. Chim. Acta*, **2003**, *356*, 365-378.

[17] H. Aghabozorg, M. Ghadermazi, J. Soleimannejad, S. Sheshmani, *Acta Cryst. E*, **2007**, *63*, m1917-m1918.

[18] a) M. Mirzaei, H. Eshtiagh-Hosseini J. T. Mague, *Acta Cryst.*, **2012**, *E68*, m174; b) Z. Derikvand, A. Nemati, A. Shokrollahi, F. Zarghampour, *Inorg. Chim. Acta*, **2012**, *392*, 362)

[19] H. Aghabozorg, N. Firoozi, L. Roshan, H. Eshtiagh-Hosseini, A. R. Salimi, M. Mirzaei, M. Ghanbari, M. Shamsipur, M. Ghadermazi, *J. Iran. Chem. Soc.*, **2011**, *8*, 992-1005.

[20] a) A. Bauza, T. J. Mooibroek, A. Frontera, *Chem. Commun.*, **2015**, *51*, 1491-1493; b) S. Roy, A. Bauza, A. Frontera, R. Banik, A. Purkayastha, M. G. B. Drew, B. M. Reddy, B. Sridhar, S. Kr. Dasa S. Das, *CrystEngComm*, **2015**, *17*, 3912-3916. c) P. Pal, S. Konar, M. S. El Fallah, K. Das, A. Bauza, A. Frontera and S. Mukhopadhyay, *RSC Adv.*, **2015**, *5*, 45082-45091; d) M. Mirzaei, H. Eshtiagh-Hosseini, M. Shamsipur, M. Saeedi, M. Ardalani, A. Bauzá, J. T. Mague, A Frontera, M. Habibi, *RSC Adv.*, **2015**, *5*, 72923-72936.

[21] G. A. Fugate. Complexation of f-Elements with Aminopolycarboxylate Ligands, Florida State University, PHD tesis, 2004.

[22] E. P. Serjeant, B. Dempsey, Ionization Constants of Organic Acids in Aqueous Soloutions, Pergamon Press, Oxford, 1974.

[23] a) E. Norkus, I. Stalnioniene, C. Crans, *Chemija (Vilnius)*, **2002**, *13*, 194-202; b) G. Anderegg, *Helv. Chim. Acta*, **1963**, *46*, 1011-1017.

[24] Z. Derikvand, M. M. Olmstead, B. Q. Mercado, A. Shokrollahi, M. Shahryari, *Inorg. Chim. Acta*, **2013**, *406*, 256.

Submitted: February 26, 2016
Accepted: April 7, 2016